The EMBO Journal (2004) 23, 1433–1440 | © 2004 European Molecular Biology Organization | All Rights Reserved 0261-4189/04
www.embojournal.org

THE EMBO JOURNAL

Myo1c is designed for the adaptation response in the inner ear

Christopher Batters[1,5], Christopher P Arthur[2,5], Abel Lin[2,5], Jessica Porter[3,5], Michael A Geeves[4], Ronald A Milligan[2], Justin E Molloy[1] and Lynne M Coluccio[3,*]

[1]Division of Physical Biochemistry, National Institutes for Medical Research, The Ridgeway, Mill Hill, London, UK, [2]Center for Integrative Molecular Biosciences, The Scripps Research Institute, La Jolla, CA, USA, [3]Boston Biomedical Research Institute, Watertown, MA, USA and [4]Department of Biosciences, University of Kent, Canterbury, Kent, UK

The molecular motor, Myo1c, a member of the myosin family, is widely expressed in vertebrate tissues. Its presence at strategic places in the stereocilia of the hair cells in the inner ear and studies using transgenic mice expressing a mutant Myo1c that can be selectively inhibited implicate it as the mediator of slow adaptation of mechanoelectrical transduction, which is required for balance. Here, we have studied the structural, mechanical and biochemical properties of Myo1c to gain an insight into how this molecular motor works. Our results support a model in which Myo1c possesses a strain-sensing ADP-release mechanism, which allows it to adapt to mechanical load.

The EMBO Journal (2004) **23,** 1433–1440. doi:10.1038/sj.emboj.7600169; Published online 11 March 2004
Subject Categories: structural biology; cell & tissue architecture
Keywords: adaptation; molecular motor; Myo1c; myosin

Introduction

The vertebrate ear consists of a series of fluid-filled chambers that contain the mechanosensitive hair cells responsible for hearing and balance. Bundles of stereocilia, which extend from the surface of these cells into the chambers, are sensitive to minute mechanical changes. The tip of each stereocilium is linked to the side of the adjacent stereocilium by an extracellular filament, or tip link, that inserts at a mechanically sensitive ion channel. Sound or motion causes the stereocilia to slide past each other. Positive displacement of the stereocilia increases tension in the tip links (or 'gating springs'), opening the channels. Negative displacement decreases tension and causes channel closure. Within milliseconds of stereociliar sliding, the channels return to their resting state in a process known as adaptation. Although Myo7a has been proposed to anchor transduction channels in auditory hair cells (Kros *et al*, 2002), there is considerable evidence that Myo1c is the adaptation motor. A complex containing multiple molecules of Myo1c crosslinks the transduction channel to the actin core of the stereocilia and mediates adaptation in vestibular cells. The complex regulates the resting tension in the tip link filament by moving up and down the actin bundle to maximise the sensitivity of the hair cell (Assad and Corey, 1992; Gillespie and Corey, 1997; Holt *et al*, 2002). To fulfil this function, the myosin is expected to have mechanochemical attributes that allow it to respond to increased or decreased strain.

A model invoking a strain-sensitive ADP release mechanism has recently been described to explain how myosins can respond to strain (Cremo and Geeves, 1998; Geeves *et al*, 2000). A strain-sensitive ADP mechanism is expected to show three characteristics: (i) a structural change associated with ADP release, which is opposed by a load on the head; (ii) a high affinity for ADP such that the free energy of ADP release is small compared to the strain energy in the load-bearing head, and (iii) weak coupling between ADP- and actin-binding such that both ADP and actin remain tightly bound to myosin (see Cremo and Geeves, 1998 and Figure 1). Actin displaces ADP from myosin and thermodynamic linkage requires that ADP will displace actin from myosin to the same degree ($K_{AD}/K_D = K_{DA}/K_A$, where the dissociation constants of actin for myosin, actin for myosin.ADP and ADP for actomyosin are K_A, K_{DA} and K_{AD}, respectively). For fast muscle myosins this coupling constant is 50–100. For myosins exhibiting enhanced strain sensitivity this is reduced to 1–10 (Cremo and Geeves, 1998). The combination of a weak coupling constant and high affinity for ADP means that work has to be carried out to displace ADP, and the long-lived A.M.D species has a high affinity for actin allowing it to bear large loads without detaching from actin.

As isolation of myosin from the ear is impractical, we have studied Myo1c purified from rat liver (Coluccio and Conaty, 1993). We used cryo-electron microscopy, single molecule mechanical methods and transient and steady-state biochemical analyses to investigate how the molecular mechanism of Myo1c is adapted to fulfil its proposed physiological role.

Results

In some myosins (e.g., smooth muscle myosin-II, Myo1a, Myo1b), there are structural and mechanical changes associated with both Pi release and ADP release (Jontes *et al*, 1995; Whittaker *et al*, 1995b; Veigel *et al*, 1999). As the conformational changes associated with ADP release are suggestive of a strain-sensing mechanism (Cremo and Geeves, 1998; Coluccio and Geeves, 1999; Geeves *et al*, 2000), we investigated whether Myo1c possesses these properties.

Cryo-electron microscopy and helical image analysis were used to calculate three-dimensional maps of Myo1c bound to F-actin in the ADP and nucleotide-free states. In the maps, the geometry of the motor domain and its interaction with actin

*Corresponding author. Boston Biomedical Research Institute, 64 Grove Street, Watertown, Boston, MA 2472-2829, USA. Tel.: +1 617 658 7784; Fax: +1 617 972 1761; E-mail: coluccio@bbri.org
[5]These authors contributed equally to the work

Received: 29 July 2003; accepted: 19 February 2004; published online: 11 March 2004

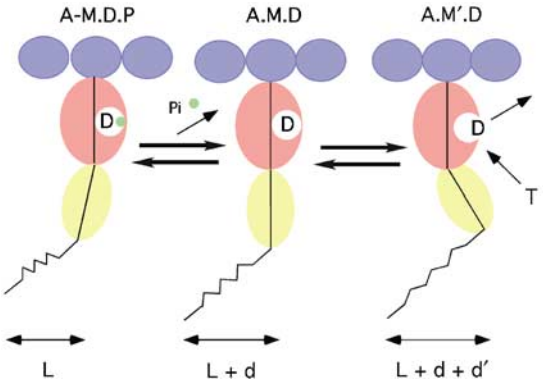

Figure 1 A strain-dependent ADP release mechanism. The cartoon depicts a myosin motor (red) attached to an actin filament (blue). Following an isometric power stroke (coupled to Pi release; A-M.D.P to A.M.D), the ADP (D) remains trapped in the nucleotide pocket of the strained myosin head. A further movement (A.M.D to A.M'.D) of the converter domain/LCBD (yellow) is required to open the nucleotide pocket and allow ADP dissociation. If such a movement of the converter domain is in the same direction as the power stroke, then the strain on the isometric motor will oppose the additional movement required. If the strain is dissipated by movement of the tail of the myosin relative to actin then the movement is not inhibited. For effective inhibition of ADP release, the free energy associated with the conformational change and subsequent ADP release must be small compared to the energy required to stretch the elastic element. In addition, the affinity of the motor for actin must remain high in the A.M.D state to prevent strain-induced detachment of the motor. Thus, a strain-sensitive ADP mechanism requires: (i) ADP-coupled movement of the converter; (ii) high affinity (i.e., low delta G) of ADP; and (iii) low coupling between ADP and actin affinities such that both remain tightly bound in the ternary complex.

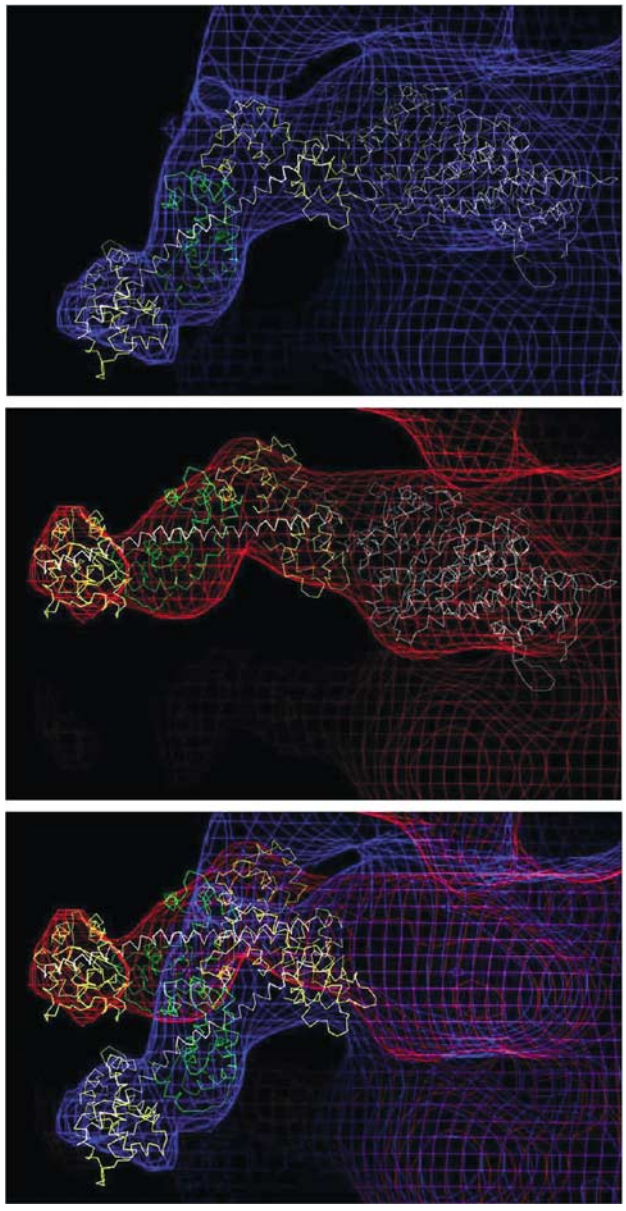

Figure 2 3D Maps of the ADP and rigour states of Myo1c calculated by cryo-EM and image analysis. In each panel, the molecular envelope of the bound myosin head is shown in chicken wire representation. The actin filament is at right running vertically, with the pointed end of the filament towards the bottom (as in Figure 6). The alpha-carbon backbone of a motor domain X-ray structure (white) has been docked into the molecular envelope. The LCBD model consists of a C-terminal heavy-chain helix (white). The calmodulin light chains are represented by three chicken skeletal muscle myosin essential light chains (yellow, green, yellow) whose positions and orientations are dictated by the spacing of the IQ motifs in the sequence. Shown are the ADP (top) and rigour (middle) states. In the bottom panel, these two 3D maps have been superimposed to show the 33° swing of the LCBD clearly. The Myo1c tail domain (235 amino acids) is not visible either because it is flexibly linked to the molecule or because of insufficient resolution in the images.

is very similar to that seen in all other myosins (Jontes *et al*, 1995; Whittaker *et al*, 1995b). At the resolution of the investigation, there are no detectable conformational changes in the motor domain between the ADP and nucleotide-free states. Distal to the motor domain, elongated density attributable to the three calmodulins of the light chain binding domain (LCBD) (Reizes *et al*, 1994; Zhu and Ikebe, 1994; Ruppert *et al*, 1995) is visualised in both states. In the nucleotide-free state (red, Figure 2), the LCBD projects outwards from the end of the motor domain. It is tilted towards the pointed end of the actin filament making an angle of $\sim 15^{\circ}$ with a line normal to the filament axis. In the ADP state (blue, Figure 2), the LCBD density is more strongly tilted ($\sim 48^{\circ}$ from the normal). Docking of an atomic model of the LCBD into the 3D map density demonstrates that the overall conformational change can be accounted for by a rigid body rotation of the LCBD about its point of origin in the motor domain (Figure 2). During the swing, the most distal region of the Myo1c molecule, the end of the LCBD, undergoes an axial movement of ~ 5 nm. These data suggest that under the unstrained conditions of the experiment, ADP bound to Myo1c prevents the molecule from completing its mechanical cycle as proposed for the myosins discussed above.

We obtained evidence for a two-step mechanical cycle in Myo1c using an optical tweezers-based single molecule mechanical transducer (see Methods and Figure 3). Individual binding events between a single, surface-immobilised myosin molecule and a single actin filament held using the optical tweezers were detected by changes in system stiffness. When myosin bound to actin, system stiffness increased about 10-fold and the thermal noise in the data was dramatically reduced. Multiple individual events, synchronised to their start and end, were then averaged to give an ensemble response (Sigworth, 1980; Veigel *et al*, 1999).

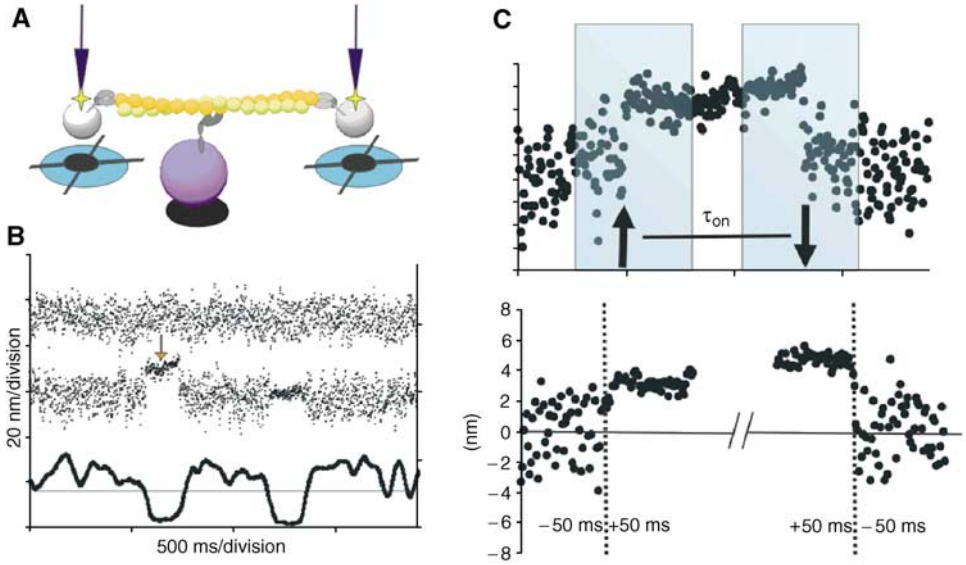

Figure 3 Powerstroke size measured using an optical-tweezers transducer. (**A**) Cartoon showing two optically trapped beads, positioned over the four-quadrant photodiode detectors. The trapped beads hold a single actin filament in the vicinity of a third surface bead coated with Myo1c. (**B**) Top trace shows the position of the optically trapped beads measured in the absence of binding interactions. Such data were used to find the distribution of bead positions caused by thermal vibration and the applied optical-tweezer oscillation. Middle trace shows data recorded parallel to the actin filament. When myosin bound to actin, the system stiffness increased about 10-fold from 0.04 pN nm^{-1} (equal trap stiffness $2\kappa_{trap}$) to 0.5 pN nm^{-1} and system noise was dramatically reduced. The arrow indicates the two phases of the actomyosin binding interaction. Reduction in the amplitude of the 100 Hz carrier signal (measured from a discrete Fourier transform of the data) is shown in the lower trace and this was used to identify the start and end of individual binding events so that event lifetimes could be accurately determined. From the distribution of bound lifetimes we found the off-rate to be 0.06 μM^{-1} s^{-1}, giving an average bound lifetime, at 20 μM ATP of 0.83 s. (**C**) The upper record shows raw data for an individual binding event (from trace B) and indicates how sections of data were extracted from the start and end of the binding event. Events were synchronised in this way and then averaged to give the ensemble response shown in the lower section (amplitude of phase 1 = 3.1 nm, phase 2 = 1.1 nm; overall displacement 4.2 nm, s.d. 1.4 nm, $n = 85$). Data shown here were recorded at 22°C, pH 7.4 and 20 μM ATP.

We found that Myo1c exhibits a two-phase powerstroke (see Figure 3B and C). The first phase produced an average movement of 3.1 nm and the second an additional movement of 1.1 nm, giving an overall displacement of 4.2 nm. This value is similar to the 3.6 nm powerstroke predicted by fluctuation analysis measurements on intact hair cell stereocilia (Frank *et al*, 2002). However, as movement generated during the second phase of the power stroke is presumably associated with ADP release, there is a discrepancy with our cryo-EM results. One possibility is that the EM data measure the most extreme position of the ADP bound state, whereas optical tweezer data measure the average of positions in that state and in the nucleotide-free rigour state. If this explanation is correct, the ADP bound state must be compliant between these extreme positions during the active cycle.

Analysis of the distribution of bound lifetimes revealed that detachment from actin was biphasic, consisting of a population of short-lived binding events (fast detachment rate) and longer-lived events (slow detachment rate). The ratio of the population amplitudes was about 2:1 (see Figure 4A and Table I). Fast events had a detachment rate constant of about 10 s^{-1} that was independent of ATP concentration. The slow event detachment rate constant was dependent on ATP concentration (up to 100 μM) giving a second order, ATP-dependent, detachment rate constant of about 0.05 μM^{-1} s^{-1}. We assume that the slow events are due to ATP binding to the A.M rigor complex, which causes dissociation of the complex (i.e., A.M + ATP → AM.ATP → A + M.ATP). As fast events were independent of ATP concentration, we suspected that this population might be caused by myosin binding to actin and then unbinding again without producing a net working stroke. To test this idea, we sorted the binding event amplitudes on the basis of their corresponding bound lifetimes and then calculated the average amplitude and average lifetime derived from consecutive blocks of 80 data values. The resulting estimates of the working stroke could then be plotted as a function of event lifetime (Figure 4B). The relationship was fitted well by an equation derived from analysis of the event lifetime distributions (see Table I and Figure 4B legend). The only additional assumption was that the fast population of events produce no movement and the slow (ATP-dependent) population produces a 4.2 nm working-stroke.

We then went on to test the effect of calcium on the mechanical behaviour of Myo1c by performing optical-trapping experiments in the presence of 77 μM free calcium (pCa 4.11). We found that the fast phase rate constant nearly doubled and the ATP-dependent slow phase became about five-fold faster; however, because the relative amplitude of the slow phase was small it was difficult to obtain accurate estimates of this rate constant. The overall effect was to make the average event lifetime much shorter (see Table I and Figure 4C). We then plotted the working-stroke estimate as a function of event lifetime (as before) and found that the movement produced by the long-lived events was now significantly increased to around 7 nm (see Figure 4C). This is now close to the range of values seen in the EM data.

Table I

	Fit to amplitude data: $A_t = (a_1/(a_1 + a_2))^* d$				Fit to lifetime data: $A_t = A_0 e^{-rt} + A_1 e^{-rt}$	
	Amplitude	Rate (s^{-1})	d (nm)		Amplitude	Rate (s^{-1})
Phase 1	135	17		20 μM, pCa 4.1	135	23
Phase 2	30	4.8	7.5		62	4.8
Phase 1	155	22		5 μM, pCa 4.1	155	16
Phase 2	30	3	7.5		65	3.8
Phase 1	80	10.5		20 μM, pCa 8.0	80	10.5
Phase 2	50	0.66	3.8		50	0.66

Additional information on the lifetime of attached states was gained from stopped-flow fluorescence spectroscopy. The pyrene fluorescence changes accompanying the dissociation of pyrene-actin from Myo1c were measured when 25 nM pyrene-actin.Myo1c, which was in a rigor state, was rapidly mixed with 50 μM–5 mM ATP. At low concentrations of ATP (50 μM; Figure 5A), the change in fluorescence could be described by a single exponential. At high concentrations of ATP, the change in fluorescence was biphasic exhibiting a slow and fast component (Figure 5B); however, the magnitude of the fast phase varied among protein preparations and represented a maximum of 30% of the total signal change. The fast phase was linearly dependent on ATP concentrations up to 1 mM (not shown; second-order rate constant = 0.014 $\mu M^{-1} s^{-1}$) and difficult to detect in the presence of Ca^{2+}. The slow phase showed a hyperbolic dependence on the ATP concentration (Figure 5C) and saturated at ~2.5 s^{-1}, requiring 680 μM ATP for 50% saturation of k_{obs} and showing no strong dependence on Ca^{2+} concentration. Extensive treatment of the sample with apyrase to remove ADP did not affect the results. The fast phase measured here is kinetically most similar to the slow phase measured in the optical trapping studies.

The simplest explanation for the biphasic nature of the ATP-induced dissociation of the acto.Myo1c complex is that previously proposed for Myo1b (Geeves *et al*, 2000). In this

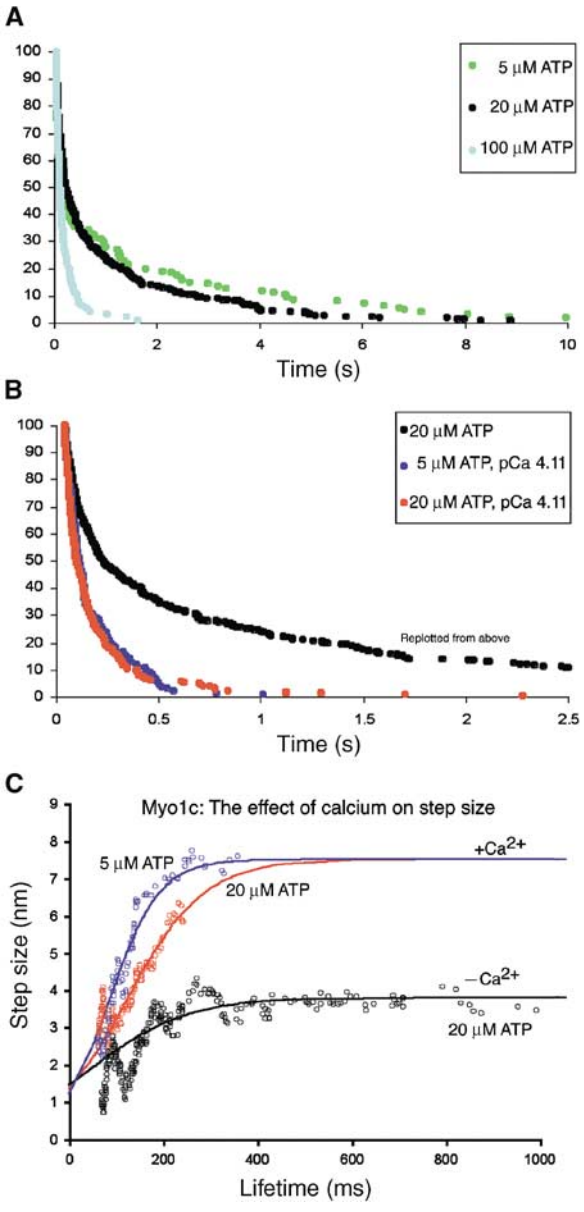

Figure 4 Lifetime measurements as a function of ATP concentration; effect of Ca^{2+}. (**A**) Scatter plot showing the lifetimes of Myo1c at 5, 20 and 100 μM ATP (n = 127, 427 and 97, respectively). Data are plotted as a cumulative distribution (e.g., data values that are less than each time point are scored and plotted at that time point) and normalised to 100%. Myo1c bound lifetime distribution exhibits a double exponential decay at all three ATP concentrations, suggesting that there are two exit routes from the attached state. Rate constants obtained by fitting a dual exponential decay indicate that there is a fast, ATP-independent phase and a slow, ATP-dependent phase (Table I). (**B**) Lifetime distribution for data obtained at pCa 4.11 with 5 and 20 μM ATP plotted as before. The data for 20 μM ATP pCa 8 are replotted from (A) for comparison. The slow phase is accelerated by about 10-fold. (**C**) The relationship between step size estimate and duration of attachment is plotted by first ranking all event amplitudes on the basis of their attached lifetime and then calculating the running average of the lifetime and step size over a window of 80 consecutive data points (each estimate of mean step size for a given time window has a s.e.m. given by s.d./$\sqrt{n}$ = 14/8.9 = 1.5 nm). The data are fitted to an equation which assumes that the fast population produces no work stroke, whereas the slow population gives a work stroke (d_{max}) of 4.2 nm in the absence of calcium and 7.2 nm in the presence of calcium. The fitted line: Work stroke$_t$ = $d_{max} \times \{Ae^{-r_s t}/(Ae^{-r_s t} + (1 - A)e^{-r_f t})\}$, where A_{slow} = relative amplitude of slow phase (%/100), d_{max} = work stroke produced by slow population, r_s = rate constant of slow phase, and r_f = rate constant of fast phase. See Table I for fitting parameters. Note the similarity of fit parameters used for lifetime data plots (A) and amplitude data plots (C).

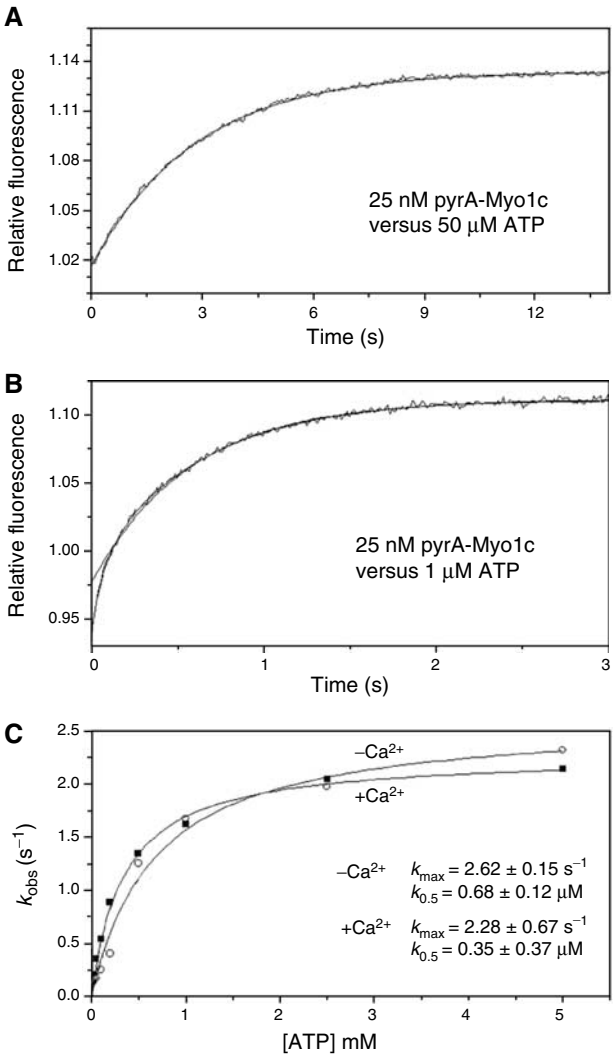

Figure 5 ATP-induced dissociation of acto-Myo1c. Pyrene-labelled acto-Myo1c (25 nM) was mixed with 50 μM–5 mM ATP. (**A**) At low ATP (50 μM) the change in fluorescence signal ($\Delta F = F_t - F_\infty$) is fit with a single exponential ($\Delta F = \Delta F_{max} \exp^{-k_{obs}t}$). (**B**) At high ATP concentration, the change in fluorescence is biphasic and exhibits a fast (1) and a slow (2) phase ($\Delta F = \Delta F_{max1} \exp^{-k_{obs1}t} + \Delta F_{max2} \exp^{-k_{obs2}t}$). The magnitude of the fast phase is variable representing 30% (maximum) of the total signal change and is linearly dependent upon ATP concentration up to 1 mM (not shown; second-order rate constant = $0.014 \times 10^6\ M^{-1}\ s^{-1}$). The fast phase is difficult to detect in the presence of Ca^{2+}. (**C**) The slow phase shows a hyperbolic dependence on ATP concentration ($k_{obs} = k_{max}[ATP]/(K_{0.5} + [ATP])$). The slow phase saturates at about 2.5 s^{-1} (k_{max}) and requires 680 μM ATP for half-saturation ($K_{0.5}$) and shows no strong dependence on Ca^{2+}. Treatment of the sample with apyrase does not affect the results.

model, myosin I exists in two conformations, one to which ATP can readily bind and one that must first undergo a conformational change allowing ADP, if present, to vacate the nucleotide pocket and ATP to bind. These two conformations are probably like the ADP and rigour states seen in the cryo-EM and mechanical studies presented here. The loss of the fast phase of the ATP-induced dissociation in the presence of Ca^{2+} is consistent with Ca^{2+} biasing the system toward the conformation that traps ADP.

Addition of 50 μM ADP to the acto.Myo1c complex was sufficient to abolish the fast phase and is consistent with the affinity of ADP to the complex being <50 μM. As the physiological concentration of ADP is in the range 10–50 μM, loss of ADP from acto.Myo1c.ADP would be unfavourable; however, if a forward directed external strain were applied to the complex, ADP release would be expected to be enhanced, i.e., work has to be carried out to release ADP. The addition of 50 μM ADP did not lead to a significant loss of total amplitude in the ATP-induced dissociation reaction. At a protein concentration of 25 nM, actin remains tightly bound to the complex (i.e., $K_D < 25$ nM); thus, there is a weak coupling between ADP binding and actin binding.

Discussion

Together, the structural, mechanical and biochemical data presented here indicate that Myo1c possesses the properties expected for a load-dependent ADP release mechanism and suggest a model of how Myo1c might mediate adaptation in the hair cell (Figure 6). In the resting state (Figure 6; *Rest*), the probability of the channels being open, P_o, is 0.1. This state is a result of the Myo1c complex moving along the actin core towards the tip of the stereocilium until the force is balanced by tension generated in the tip link, rather like a wind-up toy straining at the end of a tethered rubber rope. At this point, some myosin molecules will be unable to interact with the actin core because of the local geometry. Myosin molecules positioned with correct geometry bind at the beginning of the cycle, but are unable to proceed because of the excessive load imposed by the tension in the tip links. These molecules will remain weakly bound (yellow heads, Figure 6). It is important to note that these crossbridges are potential force generators that will play an important role in adaptation to negative displacement (see below). Myosins arrested midway through the mechanical cycle (in the strongly bound ADP conformation seen by cryo-EM) will maintain tension (blue heads, Figure 6). They are unable to release ADP because nucleotide release and mechanical events (i.e., swinging of the LCBD) are coupled. They are essentially locked in an isometric contraction and tension is maintained without nucleotide turnover. Lastly, myosins at the end of their cycle (i.e., in rigor) will bind ATP, release from actin, hydrolyse their nucleotide and, depending on the local geometry, become arrested in one of the nonrigor states just described. Fluctuation analysis on resting stereocilia of intact hair cells shows low mechanical noise (Frank *et al*, 2002) consistent with slow actomyosin cycling and predominantly stalled crossbridges.

During positive displacement (Figure 6; +), the relative movements of adjacent stereocilia generate tension in the tip links resulting in an increased probability of the ion channels being open (P_o approaches 1). This tension is also transmitted to the bound myosin molecules potentially causing reversal of the power stroke in which the LCBDs are forced into a weakly bound ADP.Pi-like conformation and the myosins detach from actin. Our optical trapping study shows that there is a significant probability of such reverse detachments from an actomyosin products state occurring and that a significant proportion of myosins bind and unbind to actin producing little or no movement. Reversal of the powerstroke is supported by muscle fibre studies (Homsher and Millar,

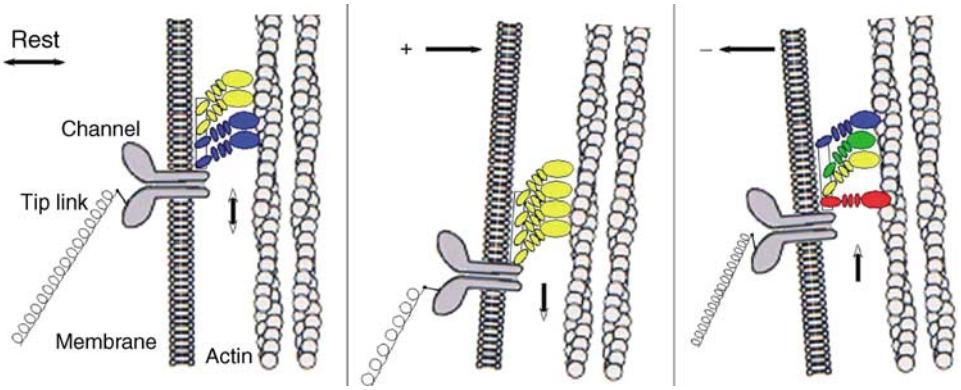

Figure 6 Schematic model for the role of Myo1c in adaptation in the hair cell. This model is adapted from Holt *et al* (2002) to depict the nucleotide state of the Myo1c molecules in the adaptation motor complex at rest (left), under positive deflection (middle) and under negative deflection (right). Red signifies Myo1c in rigour (nucleotide-free); blue, Myo1c with ADP bound; yellow, Myo1c with ADP.Pi; and green, Myo1c undergoing Pi release. The pointed ends of actin lie towards the bottom of the illustration. At rest, P_o is 0.1. The tension in the tip links is balanced by force produced by the motors. Strain is maintained by Myo1c in the ADP state. At positive deflection, P_o approaches 1.0, the channels open and the tension in the tip link causes detachment of the motor complex from the actin filament. The motor complex, still attached to the deflecting membrane, 'slips' relative to its starting position on the actin filament toward the minus end of the filament. During negative deflection, P_o approaches 0. A reduction in tip link tension reduces the strain on Myo1c allowing the motor molecules, some of which are expected to be in the strained ADP state and some at the beginning of the powerstroke, to complete the powerstroke and move up the filament to re-establish the resting state.

1990). This situation permits the channel–myosin complex to slip relative to the actin bundle, relieving tension in the tip link and permitting re-establishment of the actomyosin complexes at rest (as described in the previous paragraph) in a new position along the actin core. Recovery of the resting tension is thus accomplished by and coupled to the channels' return to the resting open probability ($P_o = 0.1$); this is called 'slipping adaptation'. The rate of slippage is controlled by a viscous drag force that is due to intermittent actomyosin interactions during slippage and is governed by the myosin detachment rate. The amplitude and kinetics of such recovery processes are likely to be a nonlinear function of load.

During the positive displacement, channel opening results in an influx of Ca^{2+}, which might be expected to play a role in adaptation. Our optical trapping studies showed that μM calcium led not only to an increase in the observed working stroke produced by actively cycling crossbridges but also to an increase in the rate at which crossbridges detached from the bound state. Our biochemical kinetic studies showed that the amplitude of the fast, forward-detachment phase became unmeasurably small. These results could be explained if the effect of Ca^{2+} were to favour the formation of the acto-Myo1c.ADP state and in addition bias the equilibrium constant backwards from the rigor state. As a consequence, the apparent rate constant for back-detachment of the bound state, the fast detachment pathway seen in optical trapping data, would be accelerated. Also, the amplitude of the fast forward-detachment route from the acto.Myo1c nucleotide-free state would be much reduced because that starting state would be depopulated. The overall effect of Ca^{2+} would be a weak modulatory role on the behaviour of Myo1c. The increased size of the maximum working stroke caused by Ca^{2+} binding to the calmodulin light chains might cause stiffening or effective lengthening of the LCBD; however, the average bound lifetime was reduced because back-detachment of bound myosins was accelerated. We expect that the net effect of Ca^{2+} is to make both the slipping and climbing adaptation processes faster, although it is difficult to define the precise effect given the multiple attached states required in our modelling.

During negative displacement (Figure 6; −), tip link tension and the probability of the ion channels being open falls (P_o approaches 0). The reduced tension would permit the potentially force-generating crossbridges to proceed through their cycle accelerating the forward transition of the previously load-bearing (ADP-containing) myosins. Structural rearrangements of bound myosins and increased actomyosin cycling would cause the myosin complex to climb towards the barbed end of the actin filaments, i.e., towards the tip of the stereocilia. Consequently, tip link tension would recover towards its resting value and the rest state of the complex would be re-established, called 'climbing adaptation'. For large displacements of the stereocilia, the rate of adaptation should correlate with the unloaded sliding velocity of Myo1c. The climbing rate predicted from physiological studies (Frank *et al*, 2002; Holt *et al*, 2002) is similar to the sliding velocity measured here in *in vitro* motility assays (Supplementary Figure 1).

Taken together, our results highlight strain-dependent ADP release as the critical attribute of the Myo1c adaptation motor. Evolutionary tuning of the coupling between myosin ATPase kinetics and LCBD conformation has resulted in a molecule capable of both movement and strain-sensitive, adaptive crosslinking. In the context of the hair cell architecture, these properties provide an elegant molecular explanation for the phenomenon of adaptation in which the exquisite sensitivity of the system is restored quickly after perturbation.

Materials and methods

Preparation of proteins and reagents

Myo1c was isolated from rat liver extracts as previously described (Coluccio and Conaty, 1993). Actin was prepared according to Spudich and Watt (1971) and, in some cases, labelled with pyrene at cys-374 (Criddle *et al*, 1985) or with rhodamine-phalloidin for motility assays (see below).

Electron microscopy

Protein handling and grid preparation were carried out at 4°C. Purified Myo1c at ~4 mg ml^{-1} was dialysed into decoration buffer (10 mM imidazole, pH 7.0, 50 mM KCl, 2 mM $MgCl_2$, 0.5 mM EGTA, 1 mM DTT, 20 μM calmodulin). F-actin (Spudich and Watt, 1971) was diluted to 50 μg ml^{-1} in decoration buffer and applied to fenestrated carbon films on EM grids. The grids were then rinsed briefly with decoration buffer and the Myo1c solution (with or without 5 mM MgADP) was then applied for 1–2 min (Whittaker *et al*, 1995b). The grids were blotted and quick frozen in liquid ethane slush. Grids were stored under liquid nitrogen.

A Gatan cryo-stage (Pleasonton, CA) was used to maintain the grids below −180°C during transfer and observation in a Phillips CM 200T FEG electron microscope. Low-dose electron micrographs (<10 e/A2 total dose) were recorded at an accelerating voltage of 120 kV, a nominal magnification of 38 000 and at defocus values ranging from −1.4 to −1.9 μm.

Image analysis

Filament images showing good optical diffraction were digitised on a Perkin-Elmer flatbed microdensitometer with a spot and step sizes of 20 μm, corresponding to 4.97 Å at the specimen. The filaments were subsequently analysed using the PHOELIX helical image processing package (Whittaker *et al*, 1995a). In short, each filament was straightened, the positions of the layer lines were determined and layer lines were extracted after correction for the effects of the contrast transfer function. Layerline data from individual filaments were then brought to the same phase origin (fitting) and averaged. The initial round of fitting and averaging was carried out using one of the data sets as the template. In subsequent rounds, the average from the previous round was used as the template. The positions of weak layerlines were refined by 'sniffing' (Morgan and DeRosier, 1992), followed by three rounds of averaging. The resolution of the final 3D maps was 25–30 Å, an estimate based on phase agreements along the layerlines.

Modelling

For docking, residues 81–791 of the skeletal myosin X-ray structure (Rayment *et al*, 1993) were used to represent the Myo1c motor domain (myosin 1s lack the N-terminal SH3 domain of skeletal and other myosins). For the LCBD, we used a single helix from the tropomyosin structure (Whitby *et al*, 1992) to represent the myosin heavy chain, and the chicken skeletal essential light chain (ELC) bound to its IQ motif (Rayment *et al*, 1993) to represent the Myo1c calmodulin light chains. We placed three ELCs along the tropomyosin helix at the precise translations and rotations dictated by the IQ spacings in the Myo1c sequence (Ruppert *et al*, 1995). Both the motor domain and LCBD models were docked manually into the 3D EM maps in O (Jones *et al*, 1991).

Single molecule studies

An optical tweezers-based force transducer built around a Zeiss Axiovert microscope (Molloy *et al*, 1995) was used to measure the mechanical transitions made by a single myosin head while attached to an actin filament (see Figure 3A). Glass microspheres (2.1 μm diameter, Bangs Labs) were applied to a coverslip surface as a suspension in 0.1% w/v nitrocellulose/amylacetate (Fullam Inc./Sigma). This was then made into a 0.1 mm-deep flow-cell (Veigel *et al*, 1998). Myo1c was diluted to a concentration of 4 μg ml^{-1} in a buffered salt solution, AB^- (Kron and Spudich, 1986) (containing in mM: 25 KCl, 25 imidazole, 4 $MgCl_2$, 1 EGTA, pH 7.4, 22°C) and allowed to bind to the coverslip surface. The surface was then blocked by flushing with 100 μl AB^-/BSA (5 mg ml^{-1}). After blocking, the solution was replaced with AB^+/CP (AB^- supplemented with, in mM: 2 creatine phosphate, 20 dithiothreitol (DTT), various [ATP]; and 1.1 mM $CaCl_2$ for the high calcium, pCa 4.11, experiments and zero added calcium for the pCa >8.0 experiments; and in mg ml^{-1}: 1 creatine phosphokinase, 0.5 BSA, 3 glucose, 0.1 glucose oxidase, 0.02 catalase (Kishino and Yanagida, 1988)). This solution also contained rhodamine-phalloidin-labelled actin filaments and 1.1 μm polystyrene beads (Sigma), which were precoated with NEM-modified myosin (Veigel *et al*, 1998). An actin filament was captured between two NEM-myosin coated polystyrene beads using optical tweezers to manipulate the beads. The actin was then held, mid-solution, in the vicinity of a third, myosin-coated, surface bead. Interactions between the suspended actin filament and the surface bound Myo1c molecules were measured at optical tweezer stiffnesses (κ_{trap}) between 0.02 and 0.04 pN nm^{-1} at 22°C. The motions of both optically trapped beads were monitored by brightfield microscopy using two, four-quadrant, photodetectors (Molloy *et al*, 1995). Data were collected (at 2 kHz sampling frequency), while a 100 nm amplitude sinewave (100 Hz) oscillation was applied to one of the laser traps. Changes in the amplitude of this signal pick-up was used as a sensitive monitor of system stiffness, hence myosin binding events.

Transient enzyme kinetics

Kinetic experiments were performed at 19.8°C in 20 mM MOPS, 100 mM KCl, 5 mM $MgCl_2$, 1 mM DTT, and 1 mM EGTA or 1 mM EGTA and 1.1 mM $CaCl_2$ at pH 7.0. All measurements were performed with a Hi-Tech Scientific SF-61 single mixing stopped-flow system using a 100 W Xe/Hg lamp and a monochromator for wavelength selection. Pyrene fluorescence was excited at 365 nm and emission detected after passing through a KV 389 nm cut-off. Tryptophan fluorescence was excited at 297 nm and observed through a WG 320 filter. The stated concentrations of reactants are those after mixing in the stopped-flow observation cell. Stopped flow data were fitted to exponentials by a nonlinear least-squares curve fit using the software Origin.

Supplementary data

Supplementary data are available at *The EMBO Journal* Online.

Acknowledgements

We thank Peter Gillespie for a critical reading of the manuscript. This work was supported by grants from the NIH (GM39155, GM61939, RR17573, GM068080), the March of Dimes Birth Defects Foundation, Medical Research Council and the Wellcome Trust, UK.

References

Assad JA, Corey DP (1992) An active motor model for adaptation by vertebrate hair cells. *J Neurosci* **12:** 3291–3309

Coluccio LM, Conaty C (1993) Myosin-I in mammalian liver. *Cell Motil Cytoskeleton* **24:** 189–199

Coluccio LM, Geeves MA (1999) Transient kinetic analysis of the 130-kDa myosin I (myr 1 gene product) from rat liver: a myosin I designed for maintenance of tension? *J Biol Chem* **274:** 21575–21580

Cremo CR, Geeves MA (1998) Interaction of actin and ADP with the head domain of smooth muscle myosin: implications for strain-dependent ADP release in smooth muscle. *Biochemistry* **37:** 1969–1978

Criddle AH, Geeves MA, Jeffries T (1985) The use of actin labelled with *N*-(1-pyrenyl)iodoacetamide to study the interaction of actin with myosin subfragments and troponin/tropomyosin. *Biochem J* **232:** 343–349

Frank JE, Markin V, Jaramillo F (2002) Characterization of adaptation motors in saccular hair cells by fluctuation analysis. *Biophys J* **83:** 3188–3201

Geeves MA, Perreault-Micale C, Coluccio LM (2000) Kinetic analyses of a truncated mammalian myosin I suggest a novel isomerization event preceding nucleotide binding. *J Biol Chem* **275:** 21624–21630

Gillespie PG, Corey DP (1997) Myosin and adaptation by hair cells. *Neuron* **19:** 955–958

Holt JR, Gillespie SK, Provance DW, Shah K, Shokat KM, Corey DP, Mercer JA, Gillespie PG (2002) A chemical-genetic strategy implicates myosin-1c in adaptation by hair cells. *Cell* **108:** 371–381

Homsher E, Millar NC (1990) Caged compounds and striated muscle contraction. *Annu Rev Physiol* **52:** 875–896

Jones TA, Zou JY, Cowan SW, Kjeldgaard M (1991) Improved methods for building protein models in electron density maps

and the location of errors in these models. *Acta Crystallogr A* **47:** 110–119

Jontes JD, Wilson-Kubalek EM, Milligan RA (1995) A 32 degree tail swing in brush border myosin I on ADP release [see comments]. *Nature* **378:** 751–753

Kishino A, Yanagida T (1988) Force measurements by micromanipulation of a single actin filament by glass needles. *Nature* **334:** 74–76

Kron SJ, Spudich JA (1986) Fluorescent actin filaments move on myosin fixed to a glass surface. *Proc Natl Acad Sci USA* **83:** 6272–6276

Kros CJ, Marcotti W, van Netten SM, Self TJ, Libby RT, Brown SD, Richardson GP, Steel KP (2002) Reduced climbing and increased slipping adaptation in cochlear hair cells of mice with Myo7a mutations. *Nat Neurosci* **5:** 41–47

Molloy JE, Burns JE, Sparrow JC, Tregear RT, Kendrick-Jones J, White DC (1995) Single-molecule mechanics of heavy meromyosin and S1 interacting with rabbit or *Drosophila* actins using optical tweezers. *Biophys J* **68:** 298S–303S, 303S–305S

Morgan DG, DeRosier D (1992) Processing images of helical structures: a new twist. *Ultramicroscopy* **46:** 263–285

Rayment I, Rypniewski WR, Schmidt-Base K, Smith R, Tomchick DR, Benning MM, Winkelmann DA, Wesenberg G, Holden HM (1993) Three-dimensional structure of myosin subfragment-1: a molecular motor [see comments]. *Science* **261:** 50–58

Reizes O, Barylko B, Li C, Sudhof TC, Albanesi JP (1994) Domain structure of a mammalian myosin I beta. *Proc Natl Acad Sci USA* **91:** 6349–6353

Ruppert C, Godel J, Müller RT, Kroschewski R, Reinhard J, Bähler M (1995) Localization of the rat myosin I molecules myr 1 and myr 2 and *in vivo* targeting of their tail domains. *J Cell Sci* **108:** 3775–3786

Sigworth FJ (1980) The variance of sodium current fluctuations at the node of Ranvier. *J Physiol* **307:** 97–129

Spudich JA, Watt S (1971) The regulation of rabbit skeletal muscle contraction. I. Biochemical studies of the interaction of the tropomyosin–troponin complex with actin and the proteolytic fragments of myosin. *J Biol Chem* **246:** 4866–4871

Veigel C, Bartoo ML, White DC, Sparrow JC, Molloy JE (1998) The stiffness of rabbit skeletal actomyosin cross-bridges determined with an optical tweezers transducer. *Biophys J* **75:** 1424–1438

Veigel C, Coluccio LM, Jontes JD, Sparrow JC, Milligan RA, Molloy JE (1999) The motor protein myosin-I produces its working stroke in two steps [see comments]. *Nature* **398:** 530–533

Whitby FG, Kent H, Stewart F, Stewart M, Xie X, Hatch V, Cohen C, Phillips Jr GN (1992) Structure of tropomyosin at 9 angstroms resolution. *J Mol Biol* **227:** 441–452

Whittaker M, Carragher BO, Milligan RA (1995a) PHOELIX: a package for semi-automated helical reconstruction. *Ultramicroscopy* **58:** 245–259

Whittaker M, Wilson-Kubalek EM, Smith JE, Faust L, Milligan RA, Sweeney HL (1995b) A 35-A movement of smooth muscle myosin on ADP release [see comments]. *Nature* **378:** 748–751

Zhu T, Ikebe M (1994) A novel myosin I from bovine adrenal gland. *FEBS Lett* **339:** 31–36